Korean J. Chem. Eng., **29**(1), 9-17 (2012)
DOI: 10.1007/s11814-011-0117-2

Dynamic simulation based fault detection and diagnosis for distillation column

Wende Tian*,†, Qingjie Guo*, and Suli Sun**

*College of Chemical Engineering, Qingdao University of Science & Technology, Qingdao, P. R. China
**School of Polymer Science and Engineering, Qingdao University of Science & Technology, Qingdao, P. R. China
(*Received 18 February 2011 • accepted 29 April 2011*)

Abstract−The model-based fault diagnosis approach is characterized by a powerful process supervision capability with a priori knowledge about the system under consideration. Nevertheless, system complexity, high dimensionality, process nonlinearity and/or lack of good data often hamper its application in chemical engineering systems. A non-steady state model based fault detection and diagnosis method for the distillation process was developed, using dynamic simulation to monitor the distillation process and identify abnormal sources when large deviations among measuring variables occur. It continuously updates the inner distillation parameters via on-line correction and predicts the trend of measuring variables and determines the existence of malfunctions simultaneously. The distillation model is dependent on transfer equilibrium, mass and heat balance, and is simulated by Euler and two-tier approach. This method was demonstrated with simulated data of a stripping tower collected from the Tennessee Eastman chemical plant simulator.

Key words: Fault Diagnosis, Distillation, Dynamic Simulation, Parameter Estimation

INTRODUCTION

A distillation column is one of most widely used unit operations in the chemical industry. Its malfunction in case of low processing capacity and/or separation efficiency can yield not only large pecuniary loss but also some hidden safety hazards. Fault diagnosis analyzes the data collected from chemical processes to determine whether a fault has occurred in the process [1]. Existing fault diagnosis methods are classified into three general categories: quantitative model-based methods, qualitative model-based methods, and process history based methods [2]. At present, fault diagnosis study for distillation column is mainly focused on the second and third methods. Generally, expert system is always combined with other methods, including fuzzy logical, neural network, and wavelet analysis, to construct a modularized hybrid fault diagnosis system for distillation column, which is able to find failure causes and give the corresponding safety precautions in a timely manner [3,4]. Artificial neural network is used as a fault diagnostic tool to represent correlation between inputs (sensor measurements) and outputs (faults) using the back propagation algorithm [5,6]. Subspace monitoring is employed as a condition monitoring tool that requires considerably fewer variables in identifying and isolating fault conditions [7]. These methods emphasize mostly the target attribute analysis, characterized by quickness and simplicity but limit analytical depth and accuracy. To overcome these weaknesses, the quantitative model-based method improves input-output, state-space and first-principles models to express internal relationships within a system, and extracts abnormal deviations through state identification, parameter estimation, parity relations, etc. [8]. In this method, extended Kalman filter (EKF), Bayesian approach, and reduced order model are usually used to represent the plant dynamics with one or more linear perturbation models [9-11].

Currently, quantitative model-based approaches for distillation columns contain the following three features. First, the fact that different steps in fault diagnosis (detection, isolation, and estimation of the magnitude of a fault) are clearly separated creates some trouble in process model selection and calculation. Second, the measured data are usually incomplete and inaccurate, so it needs to design some specific observers to deduce the values of unmeasured variables, thus leading to a weak generalization property for the chosen model. Finally, the dynamic model is limited to residual evaluation use only.

In chemical engineering, a number of applications of dynamic simulation have been performed in recent years to analyze quantum chemical molecular dynamics [12], plant start-up and shut-down [13], advanced control design [14], and data reconciliation [15]. Its rigorous mechanism model can fully reflect the inner character of a chemical process under abnormal scenarios. Based on our previous dynamic simulation studies [16-18], a non-steady state model-based fault detection and diagnosis system for distillation process is proposed in this paper. The effects of detection measure, fault type etc., are then discussed.

The purpose of this work is to evaluate the effectiveness of one single unsteady-state model for simultaneous fault detection and diagnosis. A distillation column is used to illustrate the procedure. The dynamic distillation model is summarized first. Then, its solving method is described prior to the introduction of the proposed dynamic simulation based fault diagnosis scheme. This is followed by the development of a fault detection and diagnosis scheme to estimate fault magnitude and signature. Finally, the utility of the proposed monitoring scheme is demonstrated using a simulation example, giving simulation, fault detection and diagnosis results.

NON-STEADY MODELING AND DYNAMIC SIMULATION OF DISTILLATION

1. Distillation Modeling

One distillation column is simplified as series of flash stages in

†To whom correspondence should be addressed.
E-mail: tianwd@qust.edu.cn

place of real column trays. The assumption of such a model consists of the following:

(A) The vapor-liquid phase mixes completely on a stage.

(B) The vapor-liquid phase lies in equilibrium on a stage.

(C) Heat transfers between stages quickly so heat accumulation on a stage can be neglected.

(D) Heat loss from column to environment can be neglected.

(E) Dynamic behavior of reboiler and condenser is not considered.

Compared with above equilibrium stage model, the non-equilibrium stage model assumes that the vapor-liquid equilibrium is established only at the interface between the bulk liquid and vapor phases, and employs a transport-based approach to predict the flux of mass and energy across the interface [19]. So it eliminates the need for efficiencies and HETPs (height equivalent to a theoretical plate), and is a more accurate modeling of distillation. However, the modeling and simulation with the non-equilibrium stage model is a computationally rigorous activity as it involves large number of transfer parameters and highly non-linear equations. Because the main aim of our work is to investigate how to integrate a dynamic model into fault diagnosis scheme, the equilibrium stage model is adopted here for simplicity. The near future work will focus on non-equilibrium stage model to expect a more realistic result.

If n stages and m components exist in a distillation column, then the basic equations on the *j*th stage can be derived from mass balance (Eq. (1)), phase equilibrium (Eq. (2)), normalization (Eq. (3)), and heat balance (Eq. (4)). Single stage model is depicted as Fig. 1.

$$\frac{dM_{W,i,j}}{dt} = L_{j-1}x_{i,j-1} - L_j x_{i,j} - V_j y_{i,j} + V_{j+1}y_{i,j+1} + F_j x_{F,i,j} \tag{1}$$

$$y_{i,j} = k_{i,j} x_{i,j} \tag{2}$$

$$\sum_{i=1}^{m} x_{i,j} = 1,\ \sum_{i=1}^{m} y_{i,j} = 1 \tag{3}$$

$$\frac{dH_{W,j}}{dt} = L_{j-1}h_{j-1} - L_j h_j - V_j H_j + V_{j+1}H_{j+1} + F_j h_{F,j} + q_j \tag{4}$$

Assuming vapor phase is ideal gas, phase equilibrium coefficient k in Eq. (2) can be expressed as

$$k_{i,j} = \frac{p_{i,j}^0 \gamma_{i,j}}{p_j} \tag{5}$$

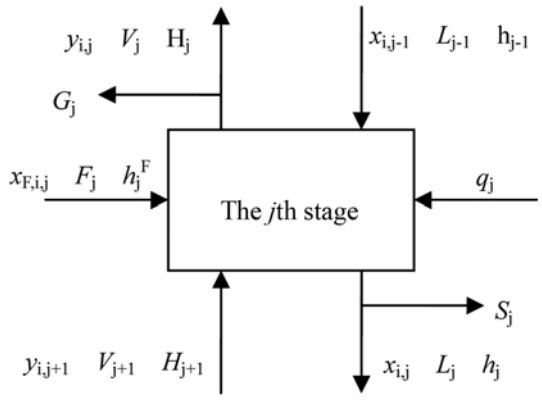

Fig. 1. Distillation stage model.

In Eq. (5), the Clausius-Clapeyron equation (Eq. (6)) is used to express the temperature dependent function of vapor pressure p^0 for simplicity. To increase computation speed, the liquid-phase activation coefficient γ in Eq. (5) is treated as constant instead of variable obtained from Wilson, NRTL, or Unifac models.

$$p_i^0 = p_{c,i} e^{hc\left(1-\frac{T_{c,i}}{T}\right)} \tag{6}$$

Besides, q in Eq. (4) represents the heat exchange rate between column stage j and environment, and is calculated by Eq. (7).

$$q_j = K_j A_j (T_{env} - T_j) \tag{7}$$

The gas flow rate V and liquid flow rate L in Eqs. (1) and (4) are calculated using Eqs. (8) and (9), respectively. As weir height on each stage is fixed, the liquid layer thickness above weir h_{OW} in Eq. (9) is determined from liquid holdup on each stage. Substituting pressure drive with exterior pressures, the modified Eq. (8) (Eq. (10)) can calculate the feed F and discharge flow (in gas or liquid phase) in Eqs. (1) and (4).

$$V_j = \frac{C_V}{M_{WV,j}} \sqrt{\rho_{V,j}(p_j - p_{j-1})} \tag{8}$$

$$L_j = 2.07 C_L \rho_{L,j} D h_{OW,j}^{1.5} / M_{WL,j} \tag{9}$$

$$F = \frac{C_F}{M_{WF}} O_{p,F} \sqrt{\rho_F \varepsilon (p_{F,in} - p_{F,out})} \tag{10}$$

Finally, the proportional-integral-differential controller (PID) algorithm is requisite in a distillation model because a real column is always running under serials of control loop. The valve regulation mode with feedback from measurement is formulated using Eqs. (11) and (12). And the derivative format of open ratio upon time (Eqs. (13)-(15)) is adopted in the distillation model to facilitate regulation algorithm in each integral loop of dynamic simulation.

$$eps = \frac{pv - sp}{hrange - lrange} \tag{11}$$

$$O_p = kp\left(eps + \frac{1}{t_i}\int_0^t eps\,dt + t_d \frac{deps}{dt}\right) \tag{12}$$

$$ek = \frac{deps}{dt} \tag{13}$$

$$ed = \frac{dek}{dt} \tag{14}$$

$$\frac{dO_p}{dt} = kp\left(ek + \frac{eps}{t_i} + ed \times t_d\right) \tag{15}$$

2. Fault Parameters

Fault is a general term used to describe a departure from an acceptable range of an observed variable that degrades process performance [2]. The source of a fault can be classified into three categories: gross parameter changes, structural changes and malfunctioning sensors and actuators. To find the particular fault source in chemical processes, one frequently needs to identify the unknown process parameters since the degradation of process performance mostly takes place as parameters change [17]. Consequently, this work aims at the faults that correspond merely to model parameters. These faults

can be further divided into two types according to the basic principles of transport phenomenon:

(A) Input flow fault. The variation of composition, temperature, and pressure of input flow brought from outside of battery limit often has an unfavorable effect on distillation operation. They can be represented by x_F in Eq. (1), h_F in Eq. (4), ε in Eq. (10) respectively. Additionally, a sticking valve can also lead to an abnormal flow rate for the pipeline with a regulating valve, so the valve open ratio O_p in Eq. (10) is another fault parameter.

(B) Heat transfer fault. The wall-type heat exchange procedure is performed in heat exchangers, formulated as Eqs. (7) and (16) where the overall heat transfer coefficient K consists of convection heat transfer resistance α in both sides of fluid, fouling resistance R_S and wall resistance b/λ.

$$\frac{1}{K}=\frac{1}{\alpha_i}\frac{d_o}{d_i}+R_{Si}\frac{d_o}{d_i}+\frac{b}{\lambda}\frac{d_o}{d_i}+R_{So}+\frac{1}{\alpha_o} \tag{16}$$

In such a heat-exchange equipment, R_{Si} and R_{So} in the right hand side of Eq. (16) always change due to heat transfer wall deposit or operation error, resulting in the decrease of K and heat transfer efficiency thereby. So, to represent the heat transfer fault, these two variables are combined into an inner model coefficient R_S as

$$R_S=R_{Si}\frac{d_o}{d_i}+R_{So} \tag{17}$$

3. Dynamic Simulation

To investigate the non-steady state behavior within a distillation column, Eqs. (1) and (4) are solved by Euler method combining constant-volume flash model, as showed in Fig. 2. In each iteration of this algorithm, mass and heat balance, temperature and pressure on each stage, and liquid and gas flow rate from each stage are calculated successively.

Unlike other dynamic simulation methods for distillation [20,21], vapor holdup is not ignored in our model, so vapor flow rates can be calculated through pressure driven mode (Eq. (8)) but not energy balances in order to reflect finely the dynamic variation of pressures. To prevent the divergence of pressure arising from the small vapor holdup, a simultaneous pressure solver and damped iteration of temperature, two useful contributions of this paper, are employed in our dynamic simulation procedure of distillation.

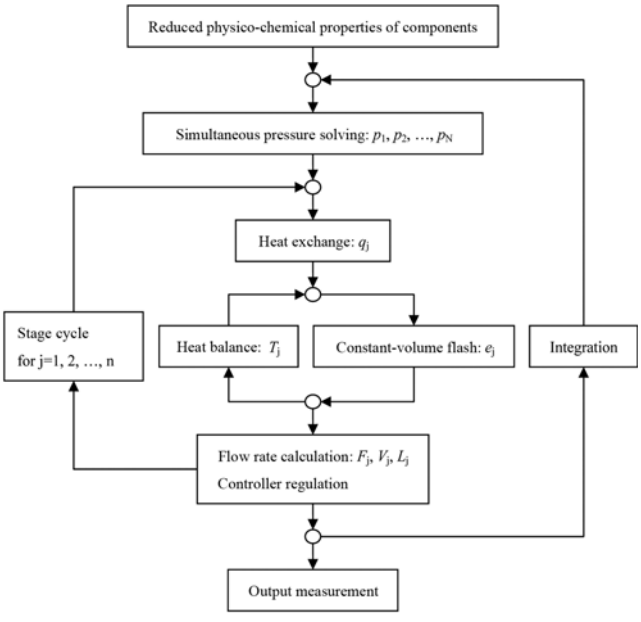

Fig. 2. Dynamic simulation algorithm of distillation.

As the core component of the whole algorithm, constant-volume flash solves vaporization ratio e (defined by Eq. (18)) through mass balance (Eq. (19)) on a stage of given volume. That is, Eq. (17) is combined with Eqs. (2), (3) and (18) to produce one implicit function of e (Eq. (20)), which is solved e by Newton method to get e.

$$e_j=\frac{M_{V,j}}{M_{W,j}} \tag{18}$$

$$M_{W,i,j}z_{i,j}=M_{V,i,j}y_{i,j}+M_{L,i,j}x_{i,j} \tag{19}$$

$$\sum_{i=1}^{m}\frac{z_{i,j}(k_{i,j}-1)}{e_j k_{i,j}+(1-e_j)}=1 \tag{20}$$

The second tier in Fig. 2 makes use of Eq. (4) to obtain temperature T. To avoid temperature iteration, linearized temperature dependent enthalpy function (Eq. (21)) is employed hereby. Additionally, a damped updating formula of temperature (Eq. (22)) is used at the end of this tier because of the significant effect of e on T. The damping factor, 150, in Eq. (23) comes from the approximate latent heat of vaporization of most chemicals because T is affected by e via phase change process.

$$H=H_0+H_1T \tag{21}$$

$$T^{(n+1)}=T^{(n)}+0.5\frac{\Delta T^{(n+1)}}{1+150\left|\Delta e^{(n+1)}\right|} \tag{22}$$

The individual pressure p_j on each stage is crucial for mass and heat balance in distillation column because its large variation can lead to an oscillation of gas flow rates and a divergent simulation for the whole column. Therefore, we incorporate a simultaneous pressure solver prior to stage iteration to solve this problem. First, Eq. (8) is linearized and substituted into Eq. (1). Second, thus obtained Eq. (1) is rearranged into a form with pressures on its left hand side. Finally, the converted equations with stage indices are constructed into a matrix (Eqs. (23)-(28)), which is solved by Gaussian elimination method.

$$\begin{pmatrix} b_1 & c_1 & & & \\ a_2 & b_2 & c_2 & & \\ & a_3 & b_3 & c_3 & \\ & & \cdots & & \\ & & & a_N & b_N \end{pmatrix}\mathbf{p}=\begin{pmatrix} d_1 \\ d_2 \\ \vdots \\ d_N \end{pmatrix} \tag{23}$$

$$a_j=-K, \text{ for } j>1 \tag{24}$$

$$b_j=\begin{cases} K+\dfrac{Vol_j}{RT_j e_j dt}, & j=1 \text{ or } n \\ 2K+\dfrac{Vol_j}{RT_j e_j dt}, & \text{otherwise} \end{cases} \tag{25}$$

$$c_j=-K, \text{ for } j<n \tag{26}$$

$$d_j=\begin{cases} F_j-(L_j+S_j)-G_j+\dfrac{M^0_{W,j}}{dt}-K\rho_{Lj}g(h_W+h_{OW,j}),\ j=1 \\ F_j+L_{j-1}-S_j-G_j+\dfrac{M^0_{W,j}}{dt}+K\rho_{Lj}g(h_W+h_{OW,j-1}),\ j=n \\ F_j+L_{j-1}-(L_j+S_j)-G_j+\dfrac{M^0_{W,j}}{dt}+K\rho_{Lj}g(h_{OW,j-1}-h_{OW,j}),\ \text{otherwise} \end{cases} \tag{27}$$

$$\mathbf{p}=(p_1p_2\cdots p_N)^T,\ K=\frac{C_V}{\rho_{Vj}} \tag{28}$$

The outmost tier in Fig. 2 executes a numerical algorithm of ordinary differential equations (ODEs) (1) and (4). In practice, Runge-Kutta and Euler methods are frequently used ODEs algorithms. The former comparatively has high integral accuracy but low speed, and requires multiple derivative computations in one integral step. But the derivative computation is time-consuming in practice due to the large number of ODEs in the distillation model. Therefore, improved Euler method (Eq. (29)) is selected in this work as the integral algorithm to increase computation speed for fault diagnosis, where h is the sampling interval time and f denotes one order derivative function.

$$\mathbf{x}_{n+1}=\mathbf{x}_n+\frac{h}{2}[f(t_n,\mathbf{x}_n)+f(t_{n+1},\ \mathbf{x}_n+hf(t_n,\mathbf{x}_n))] \tag{29}$$

DYNAMIC SIMULATION BASED FAULT DIAGNOSIS

1. Fault Diagnosis Procedure

Fig. 3 depicts the fault diagnosis procedure on the basis of the dynamic simulation given in the previous section. The fault detection step is carried out first, in which dynamic simulation output is compared with the local history data to decide whether the current state of the real process complies with its theoretical prediction (through Q statistic). If the real process data agree with those from theoretical prediction, meaning that the real process is normal, only continuous inspection is needed in the next cycle. If the real process data disagree with those from theoretical prediction, the real process is deemed as out of work and trouble shooting is needed in the next step. Because the external faults usually result from abnormal changes of internal model parameters, fault diagnosis will proceed with on-line correction of these parameters. Finally, the trajectory of obtained parameters is saved and analyzed to retrieve the basic causes under current faults, while the process is still under the supervision of the fault detection and diagnosis system.

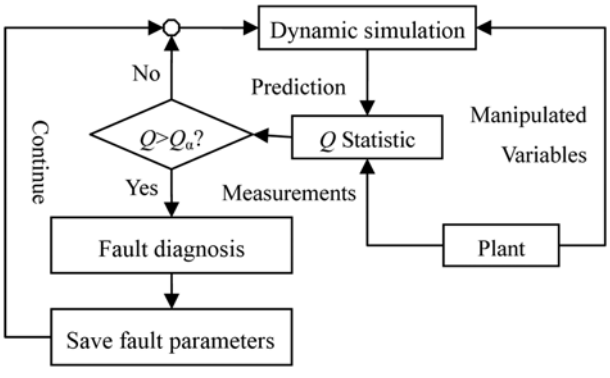

Fig. 3. Steps involved in fault diagnosis.

Owing to the inconsistent time delay of process and control loop between mathematical model and plant, not all the PID controllers (Eqs. (11)-(14)) need be included in the dynamical simulation step in Fig. 3. Only those controllers that are heavily affected by systemic dynamic characteristics should be taken into consideration. Other controllers which are mainly depending on environment condition will be bypassed and set their valve open ratios (O_p in Eq. (10)) directly from data collection of real plant.

2. Fault Detection

The on-line data collected from the process is converted into a few meaningful characteristics, which in some way represent the state or behavior of the process. If one or more characteristics deviate beyond their acceptable range, the system is regarded as abnormal. The goal of process monitoring is to develop characteristics that are maximally sensitive and robust to all possible faults. However, all faults occurring in a process are unlikely to be effectively detected and diagnosed with only a few characteristics since each characteristic represents a fault in a different manner [22]. To clarify the application of dynamic simulation in fault diagnosis, a single statistic variable Q, defined in Eq. (32), is adopted in this work for fault detection purpose. Other characteristics will be designed and introduced in our future work to meet the reliability and accuracy requirements of fault diagnosis. To get the Q statistic, simulation values of measurement are subtracted by their collection values at first (Eq. (30)), and scaled in the standard manner secondly to eliminate the effect of modeling bias and variable magnitudes on fault detection. That is, the sample mean at the normal case was subtracted from above differences and then divided by their standard deviation at the normal case (Eq. (31)).

$$\mathbf{r}=\mathbf{y}_{meas}-\mathbf{y}_{sim} \tag{30}$$

$$\mathbf{r}^*=\frac{\mathbf{r}-\bar{\mathbf{r}}}{\sigma_r} \tag{31}$$

$$Q=\mathbf{r}^{*T}\mathbf{r}^* \tag{32}$$

Assuming measured values $\mathbf{y}$ are randomly sampled from a multivariate normal distribution, and the sample mean vector $\bar{\mathbf{r}}$ and covariance matrix σ_r for normal case are equal to their actual values respectively, then the Q statistic follows a chi-square distribution with m degrees of freedom and its threshold can be determined as follows

$$Q_\alpha=\chi^2_\alpha(m) \tag{33}$$

3. Fault Diagnosis

Because the fault diagnosis makes use of a mechanism model about state space in a chemical process, the meaningful state changes will facilitate the fault isolation and estimation once Q exceeds its threshold. With time elapsing, the condition of a distillation column deviates from its optimal operating point due to a several reasons like concentration change, pressure loss, and temperature fluctuation. These reasons can be described by the fault parameters in the model of Section 2. The fault parameter vector θ, which elements are described in Section 2.2, is defined by Eq. (34). Accordingly, only through continuous model correction using real-time data collection can the coincidence between model and distillation be guar-

anteed. Such an updating process is implemented via parameter estimation, which is a kind of least square method (LSQ) in essence (Eq. (35)). The constraint in Eq. (35) is the input-output format of Eqs. (1)-(28). LSQ algorithm uses subspace trust region method. Fault parameter estimations at time t are saved as the initial values of LSQ at time t+1 to reduce optimization load and guarantee its convergence.

$$\theta=(x_F\ h_F\ \varepsilon\ O_p\ R_S)^T \tag{34}$$

$$\min_{\theta(t)} Q(t) \tag{35}$$

s.t. $\mathbf{y}(t)=f(\mathbf{u}(t), \omega(t), \mathbf{x}(t), \theta(t))$

CASE STUDY

The proposed dynamic simulation-based fault detection and diagnosis method is applied to the stripper of a Tennessee-Eastman progress (TEP) simulator [20] to test its feasibility under different faults.

1. Stripper Description

The stripper process is shown in Fig. 4. The condensed components, mainly components G and H, are pumped to the stripper top. Stream C, mainly components A and C, flows into the stripper bottom to remove the remaining reactants from the top feed. The products G and H from the bottom of the stripper are pumped to a downstream process which is not included in this process, while non-converted reactants, inert component, and byproduct leave the stripper from top.

The simulation code of TEP allows 21 preprogrammed major process faults, but only 6 faults among them are relative to the stripper (see Table 1). The training and testing data sets for each fault consisted of 500 and 960 observations respectively, with a sample interval of 3 minutes. Each simulator data set starts with no faults, and the faults are introduced at 1 and 8 hour for the training and testing data sets, respectively. The stripper has 12 measurements and 4 manip-

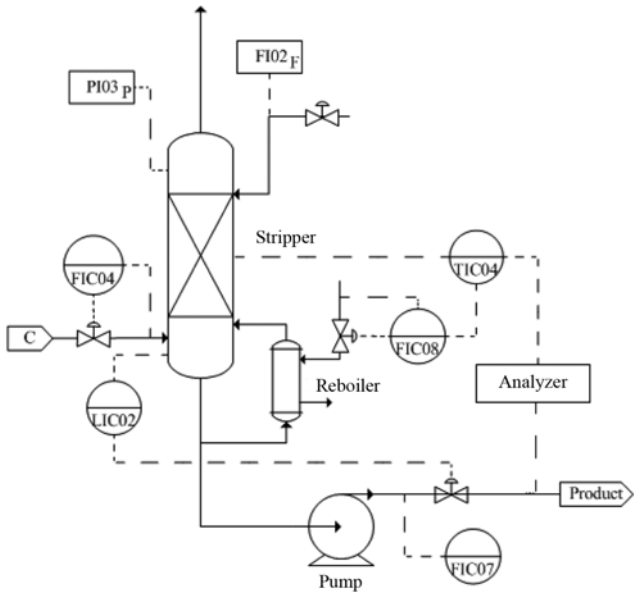

Fig. 4. Diagram of TEP stripper.

Table 1. Process faults for the stripper in TEP simulator

Fault number	Description	Type
IDV(1)	A/C composition ratio in stream 4 with constant B composition	Step
IDV(2)	B composition in stream 4 with constant A/C composition ratio	Step
IDV(7)	Header pressure loss of stream 4-reduced availability	Step
IDV(8)	A, B, C composition of stream 4	Random variation
IDV(10)	Temperature of stream 4	Random variation
IDV(21)	The valve for stream 4 was fixed at the steady state position	Step

Table 2. Parameters in the stripper model

Parameter	Value							
Diameter, m	1.4							
Integration step, s	1.0							
Coefficients in Eq. (7) for reboiler	K, kJ/(m^2·K)		S, m^2					
	290.0		14.2					
Coefficients Eq. (14) for level controller	kp, h^{-1}		t_i, s		t_d, s			
	−0.0231		50.0		0			
	A	B	C	D	E	F	G	H
Coefficient hc in Eq. (6)	6.3	5.9	5.9	4.5	3.6	3.6	2.1	1.7
γ in Eq. (5) for the 2nd stage	1	1	1	1.3	9.5	11.1	0.6	0.6
H_0 of gas enthalpy in Eq. (18), kJ/kmol	0	0	0	64685	50243	54382	68113	80392
H_1 of gas enthalpy in Eq. (18), kJ/kmol	29.2	51.8	29.4	59.2	86.02	96.96	44.14	47.43
H_0 of liquid enthalpy in Eq. (18), kJ/kmol	−8851.8	−8851.8	−8851.8	0	0	0	0	0
H_1 of liquid enthalpy in Eq. (18), kJ/kmol	43.4	43.4	43.4	245.12	191.82	213.6	158.10	186.2

ulated variables in all.

2. Stripper Simulation

For the stripper having only one temperature measuring point, the stage number is simplified as 3 and the 2nd stage is responsible for the temperature output. The program is coded in Matlab software, and Table 2 lists all the model parameters appearing in Eqs. (1)-(28). Figs. 5 and 6 show the simulation results of column top temperature and bottom concentration of E at the base case. The coincidence of simulation values with measured ones indicates that the dynamic model can produce the non-steady variation of distillation column correctly.

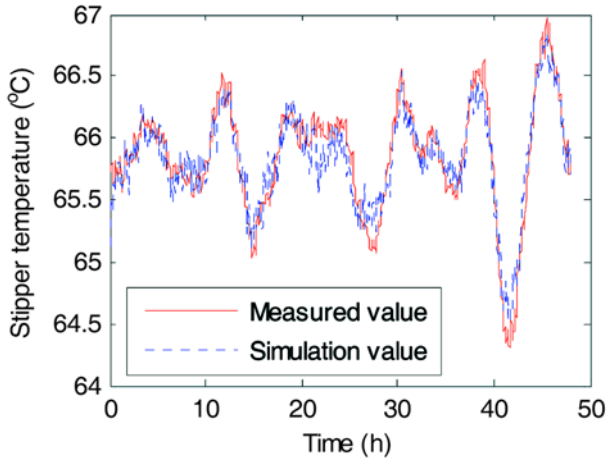

Fig. 5. Simulation result of stripper temperature.

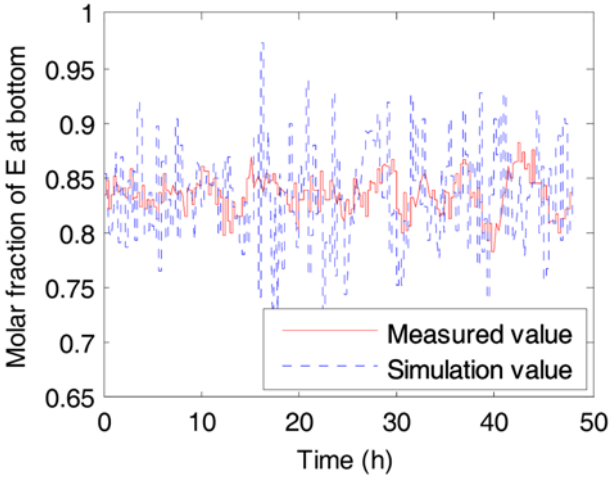

Fig. 6. Simulation result of E concentration.

3. Fault Detection of Stripper

Table 3 lists all the mean values ($\bar{\mathbf{r}}$ in Eq. (31)) and standard deviations (σ_r in Eq. (31)) of 12 observable variable residuals through dynamic simulation at base case.

Q statistic is calculated using the data in Table 3 for fault detection. Fig. 7 illustrates Q variation for fault 1 as an example. It shows apparently that the system becomes abnormal from 8 h with its state changing greatly. The given Q statistic is therefore suitable for system state representation, and facilitates fast fault detection due to its low computation load.

4. Fault Diagnosis of Stripper

Figs. 8 and 9 describe the movement of stripper temperature and E concentration of underflow under fault 7, respectively. Fault 7 occurs at 8 h when an abruptly reduced differential pressure of C

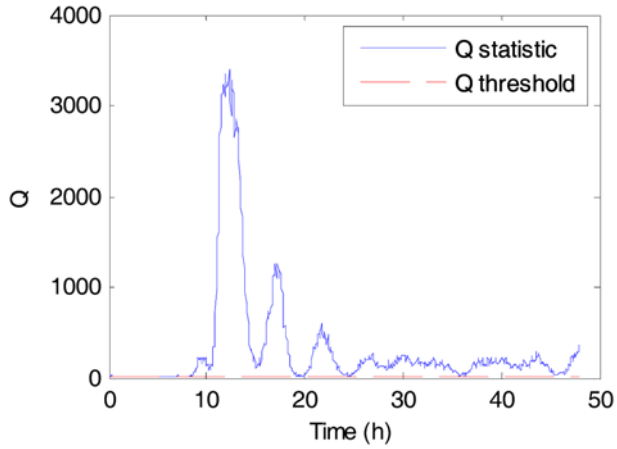

Fig. 7. Q variation under fault 1.

Table 3. Standardized Residual Parameters of Observable Variables

Variable	Residual mean	Standard deviation of residual
Flow rate of C stream, kscmh*	−0.002	0.224
Flow rate of top feed, m^3/h	−3.535	2.560
Stripper level, %	0.012	1.459
Stripper pressure, kPag	2.181	15.146
Flow rate of stripper underflow, m^3/h	0.436	2.910
Stripper temperature, °C	0.016	0.162
Flow rate of reboiler steam, kg/h	0.080	2.066
D concentration of stripper underflow, mol%	−0.003	0.010
E concentration of stripper underflow, mol%	0.001	0.049
F concentration of stripper underflow, mol%	−0.002	0.012
G concentration of stripper underflow, mol%	0.066	0.502
H concentration of stripper underflow, mol%	−0.030	0.558

*kscmh=thousand standard cubic meters per hour

stream reduces its flow rate and then degrades the stripping effect. Furthermore, Figs. 8 and 9 also present simulations value changes with diagnosis (simulation values 1) and without diagnosis (simulation values 2) simultaneously. It can be seen that measured values change greatly due to system malfunction at 8 h, and then fault diagnosis is activated to take a close tracking on measured values with their simulation values. Clearly, a large deviation between measured and simulation values appears if no fault diagnosis algorithm is incorporated.

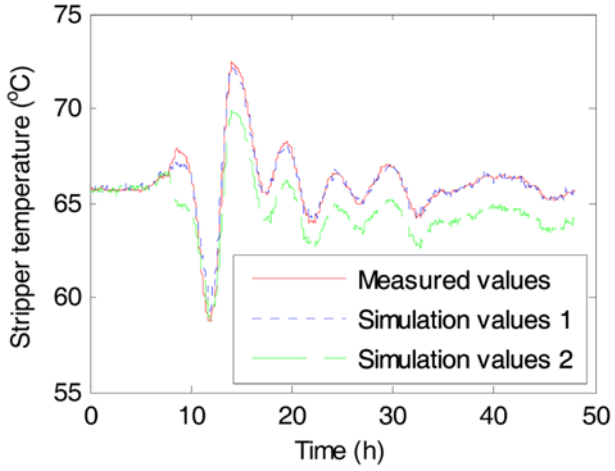

Fig. 8. Stripper temperature changes under fault 7.

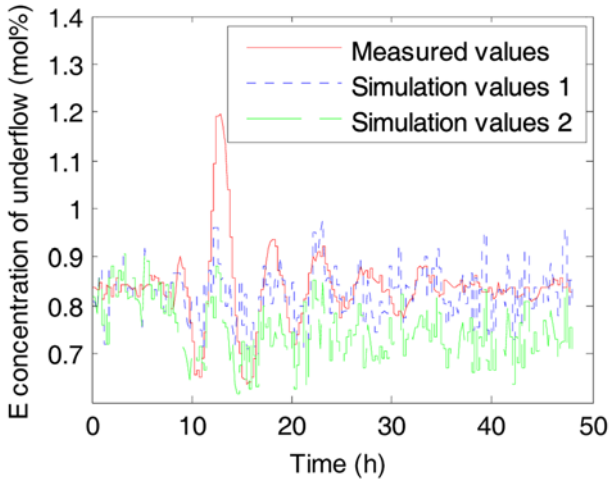

Fig. 9. E concentration of underflow under fault 7.

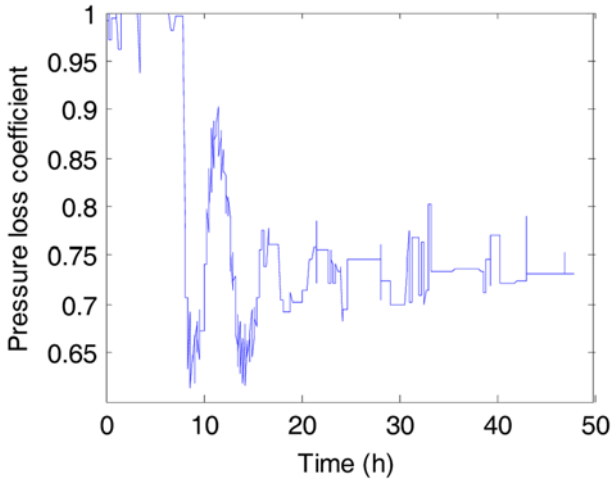

Fig. 10. Trajectory of identified fault parameter in stripper.

Fig. 10 gives the fault diagnosis result under fault 7, i.e., change of pressure loss represented by coefficient ε (defined in Eq. (10)) of C stream. As shown in Fig. 10, ε decreases greatly after 8 h and approaches 0.73 gradually. This fact says the emerging abnormal state from 8 h is caused by the decrease of ΔP. It also illustrates that our diagnosis algorithm is able to infer the change of meaningful fault parameters and assists in determining base fault reason and its level in practice.

The above-mentioned case study explains that our diagnosis algorithm is valid for step style faults. Next, a case study of fault 8 is given to explain its feasibility for random style faults. In fault 8, the composition of C stream (A, B, C concentration) changes randomly from 8 h. The introduced indeterminate fluctuation of measured values makes diagnosis work more difficult.

Figs. 11 and 12 are the diagnosis results for fault 8. Fig. 11 in-

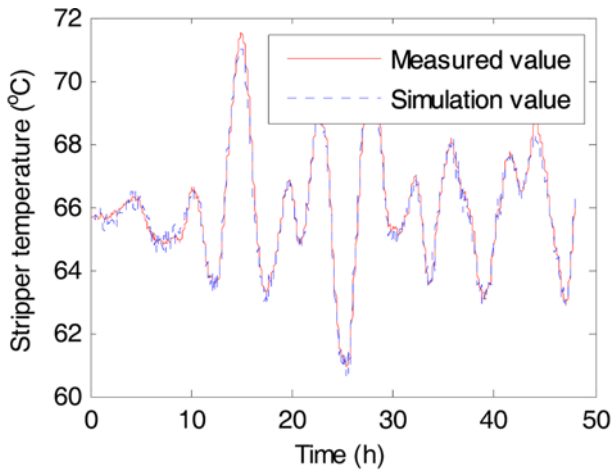

Fig. 11. Stripper temperature change under fault 8.

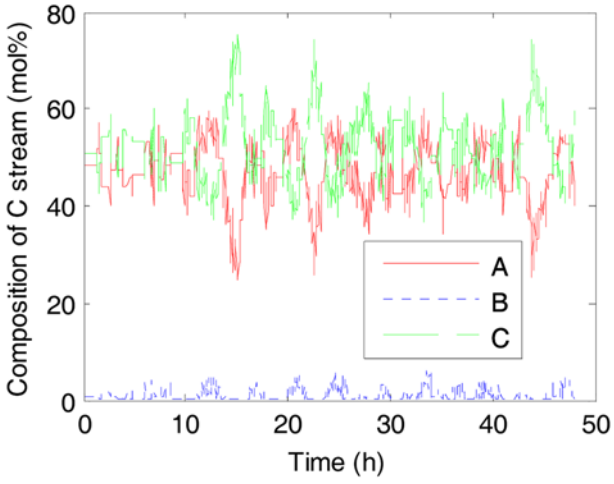

Fig. 12. Diagnosis result of fault 8.

dicates that our diagnosis algorithm well tracks the change of measured values as before. As expected, Fig. 12 clearly illustrates that diagnosis gives a continuously changing concentration of C stream. All these findings demonstrate that the present algorithm is valid for random style faults as well.

Additionally, the above diagnosis process depends largely on a sufficiently great change of fault parameters. This means the measured values should be sensitive to fault parameters. If they are insensitive, system noise may conceal the real change of fault parameters. The following case study based on fault 1 explains such a problem.

Figs. 13 and 14 show the diagnosis result under fault 1. The simulation values 1 and 2 represent simulation value changes with diagnosis and without diagnosis, respectively. In fault 1, the concentration of inertia component B keeps constant and the component ratio of A to C decreases. It can be observed from Fig. 13 that measured values are always close to simulation values with or without diagnosis algorithm. This means the concentration change of A and C plays a weak role on process output. Moreover, Fig. 14 shows an unchanged concentration of A, and means the diagnosis algorithm did not find the abnormal reason correctly. Decreasing A concentration will lead to an increasing feed rate to the outer reactor, which caused high reactor level resulting in a low flow rate of C stream afterwards. Finally, the stripper will adaptively adjust its temperature to a high value to maintain its product quality. Therefore, we cannot find such an amplification effect with mere diagnosis on the stripper, and naturally fail to determine the abnormal reason. Diagnosis on a larger system extended from the stripper is helpful to solve this problem. But the diagnosis algorithm becomes ineffective with the system scale increasing. Better performance is expected from combining the above algorithm with such knowledge-based diagnosis methods as signed direction graph (SDG), expert system, etc.

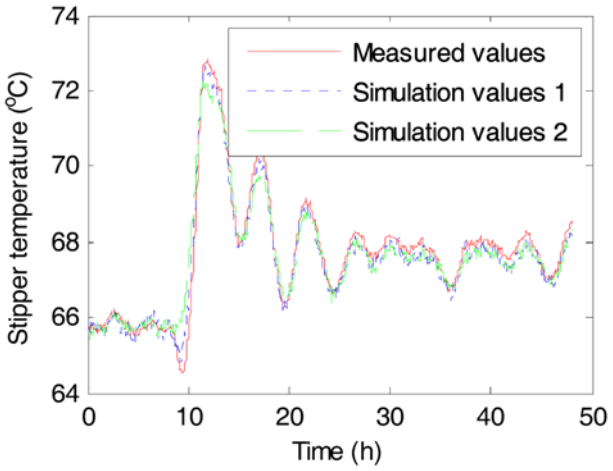

Fig. 13. Stripper temperature change under fault 1.

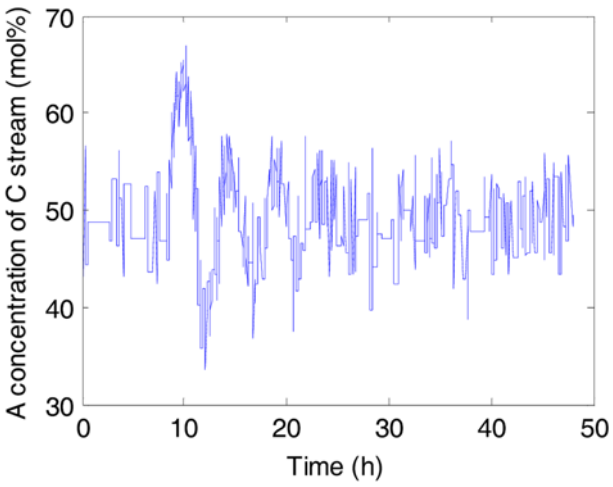

Fig. 14. Diagnosis result of fault 1.

CONCLUSIONS

One dynamic simulation-based diagnosis process for distillation is proposed in this paper. It utilizes mechanism model to simulate measured value changes before and after abnormal occurrence, thus realizing model correction and fault diagnosis equally. The simultaneous pressure solver and damped updating formula of temperature are indispensable to avoid divergence of pressures and temperatures in dynamic simulation of distillation. One important step in tracking dynamic measured values is to determine whether a fault occurs and what the base reason behind it is. The residual between the real process data and its dynamic simulation prediction is scaled as single Q statistic to simplify fault detection. And the implementation of fault diagnosis relies on the parameter correction result through a kind of least square method. The case studies based on the stripper in TEP demonstrate that our method is valid for both step and random style fault, but needs supplementing by other methods for low sensitivity fault.

Due to the modeling complexity and measurements available, this approach is limited to the fault associated with one fault parameter. Furthermore, if a fault is associated with many fault parameters, the least square method utilized in this approach may give a confusing result when converging to a local minimum. So, future research should focus on the dynamic modeling improvement and the robustness of this approach for large-scale systems.

NOMENCLATURE

A : heat transfer area [m^2]
b : wall thickness [m]
C : flow rate coefficient
d_i, d_o : inside and outside diameter of tube [m]
D : column diameter [m]
e : vaporization ratio
eps : normalized control error
E : liquid contraction coefficient (normally equals unity)
F : feed flow rate into a tray [$mol \cdot s^{-1}$]
g : acceleration of gravity [$m \cdot s^{-2}$]
G : vapor siding flow rate [$mol \cdot s^{-1}$]
h : enthalpy of feed flow into a tray or liquid flow leaving a tray [$J \cdot mol^{-1}$]
hc : constant of Clausius-Clapeyron equation
h_{OW} : liquid layer thickness above weir on a tray [m]
hrange : upper limit of measurement
H : enthalpy of whole holdup in a tray or vapor flow leaving a tray [$J \cdot mol^{-1}$]

k : phase equilibrium constant
kp : gain factor of controller
K : overall heat transfer coefficient, kJ/(m^2·K)
l_W : weir length on a tray[m]
lrange : low limit of measurement
L : liquid flow rate leaving a tray [mol·s^{-1}]
L_h : liquid volumetric flow rate leaving a tray with weir height h [mol·s^{-1}]
m : variable number
M : holdup in a tray [mol]
M_W : molecular weight [kg/kmol]
n : sampling number
O_p : valve open ratio
p : pressure [Pa]
pv : present value of measurement
q : heat transfer rate between a tray and environment [W]
Q : squared prediction error statistic
r : residual vector between measured and simulation values
r* : scaled residual vector
R_{Si}, R_{So} : inside and outside fouling resistance of tube [m^2·K·W^{-1}]
sp : set point
S : liquid siding flow rate [mol·s^{-1}]
t : time [s]
t_i : integration time constant [s]
t_d : differential time constant [s]
T : temperature [K]
u : control variable vector
V : vapor flow rate leaving a tray [mol·s^{-1}]
Vol : vapor volume on a stage [m^3]
x : composition of liquid flow or feed flow [mol·mol^{-1}]
x : state vector
y : system output vector
y : composition of vapor flow [mol·mol^{-1}]
z : composition of overall holdup in a stage [mol·mol^{-1}]
σ_r : standard deviation of residual vector
ΔP : differential pressure [Pa]
θ : fault parameter vector
ε : pressure loss coefficient
ρ : density [kg·m^{-3}]
α_i, α_o : convection heat transfer inside and outside of tube [W·m^{-2}·K^{-1}]
λ : thermal conductivity [W·m^{-1}·K^{-1}]
γ : liquid-phase activation coefficient
ω : disturb vector
χ^2_α : upper 100 α% critical point of chi-square distribution

Subscripts
c : critical properties
F : feed
i : component index
in : source
j : tray index
L : liquid
meas : measured value
W : whole
sim : calculated value
V : vapor
α : confidential level

Superscripts
F : feed
out : destination
0 : saturated vapor

ACKNOWLEDGEMENT

The authors gratefully acknowledge financial support provided by Shandong Natural Science Foundation (grant number: ZR2009BM 033).

REFERENCES

1. H. K. Min and K. Y. Chang, *Korean J. Chem. Eng.*, **25**(5), 947 (2008).
2. V. Venkatasubramanian, R. Rengaswamy, K. Yin and S. N. Kavuri, *Computers Chem. Eng.*, **27**, 293 (2003).
3. Y. F. Ding, W. D. Xu and F. Pan, *Computer Eng.*, **30**(23), 171 (2004).
4. J. Koo, S. Kim, G. Kim, Y. H. Kim and E. S. Yoon, *Korean J. Chem. Eng.*, **26**(6), 1476 (2009).
5. Y. Chetouani, *Int. J. Reliability Safety.*, **4**, 265 (2010).
6. M. H. David, *Korean J. Chem. Eng.*, **17**(4), 373 (2000).
7. D. Lieftucht, M. Völker, C. Sonntag, U. Kruger, G. W. Irwin and S. Engell, *Control Eng. Pract.*, **17**(4), 478 (2009).
8. C. K. Yoo, D. S. Kim, J. H. Cho, S. W. Choi and I. B. Lee, *Korean J. Chem. Eng.*, **18**(4), 408 (2001).
9. A. Arpornwichanop, O. Kittisupakorn and M. A. Hussain, *Korean J. Chem. Eng.*, **19**(2), 221 (2002).
10. A. P. Deshpande and S. C. Patwardhan, *Ind. Eng. Chem. Res.*, **47**(17), 6711 (2008).
11. S. Manuja, S. Narasimhan and S. Patwardhan, *Canadian J. Chem. Eng.*, **86**(4), 791 (2008).
12. K. T. Lu and K. L. Tung, *Korean J. Chem. Eng.*, **22**(4), 512 (2005).
13. X. T. Yang, Q. Xu, C. Y. Zhao, K. Y. Li and H. H. Lou, *Ind. Eng. Chem. Res.*, **48**(20), 9195 (2009).
14. S. Kim, K. S. Lee and Y. M. Koo, *Korean J. Chem. Eng.*, **22**(6), 830 (2005).
15. F. Ali, M. Z. Arjomand and B. B. Ramin, *Korean J. Chem. Eng.*, **25**(5), 955 (2008).
16. W. D. Tian, B. Wan and F. Yao, *J. Beijing University of Chemical Technology*, **28**(1), 6 (2001).
17. W. D. Tian and S. L. Sun, *Chinese J. Process Eng.*, **7**(5), 952 (2007).
18. W. D. Tian, S. L. Sun, C. L. Wang and C. K. Li, *Dynamic modeling and abnormal simulation of rectifying tower*, Proceedings of the 8th World Congress on Intelligent Control and Automation, Jinan, China (2010).
19. M. K. Amit, S. K. Ravindra, M. M. Kannan and M. M. Sanjay, *Computers Chem. Eng.*, **32**(10), 2243 (2008).
20. H. K. Young, *Korean J. Chem. Eng.*, **17**(5), 570 (2000).
21. G. Jignesh, R. Gabriel, K. Achim, S. Frank and S. Kai, *Clean Technol. Environ. Policy*, **10**(3), 245 (2008).
22. L. H. Chiang, E. L. Russel and R. D. Braatz, *Fault detection and diagnosis in industrial systems*, China Machine Press, Beijing (2003).